Applied Catalysis B: Environmental 90 (2009) 175–183

Contents lists available at ScienceDirect

Applied Catalysis B: Environmental

journal homepage: www.elsevier.com/locate/apcatb

# Catalytic reduction of *N*-nitrosodimethylamine with nanophase nickel–boron

Andrew J. Frierdich, Claire E. Joseph, Timothy J. Strathmann *

*Department of Civil and Environmental Engineering and Center of Advanced Materials for the Purification of Water with Systems, University of Illinois at Urbana-Champaign, 3209 NCEL, MC-250, Urbana, IL, 61801, United States*

ARTICLE INFO

*Article history:*
Received 29 May 2008
Received in revised form 8 October 2008
Accepted 3 March 2009
Available online 17 March 2009

*Keywords:*
NDMA
Nickel–boron
Disinfection byproducts
Hydrogenation
Water treatment

ABSTRACT

Recent work by the authors shows that toxic *N*-nitrosamines, widely detected in disinfected wastewater and drinking water and recalcitrant towards conventional treatment processes, can be rapidly reduced to less hazardous products by treatment with hydrogen and Raney nickel catalysts. Unfortunately, Raney Ni catalysts are pyrophoric when dry and are readily deactivated when exposed to air, severely limiting their application for water treatment. In this work, a non-pyrophoric and air-tolerant nickel–boron (NiB) catalyst is described, and its reactivity with *N*-nitrosodimethylamine (NDMA) is quantified. The catalyst, prepared by aqueous reduction of $NiCl_2$ with $NaBH_4$, has an elemental composition of 85 wt.% Ni and 7 wt.% B. Nanophase primary catalyst particles are formed and aggregate in micrometer-sized assemblies in solution. The catalyst has a specific surface area of 18 $m^2\ g^{-1}$, and the surface contains Ni(0) and B in a mixture of oxidation states (0/+III). Kinetic studies show that NDMA is rapidly reduced via hydrogenation to dimethylamine and ammonia in $H_{2(g)}$-saturated ($P_{H_2} = 1$ atm) aqueous NiB suspensions, with mass- and surface area-normalized first-order rate constants of $29.5 \pm 2.4$ L $g_{Ni}^{-1}\ h^{-1}$ and $1.38 \pm 0.11$ L $m_{cat}^{-2}\ h^{-1}$, respectively. Although the mass-normalized rate constant is less than that measured for Raney Ni, the surface area-normalized rate constant is greater, suggesting higher intrinsic reactivity of the NiB surface if the availability of surface sites for NDMA reactions on either catalyst surface is not significantly affected by aggregation of the catalyst nanoparticles. Kinetic studies show that reactivity of the NiB catalyst with NDMA is unaffected by solution pH and extended pre-exposure of the dry catalyst to air (Raney Ni is immediately deactivated by exposure to air). The NiB catalyst is also more tolerant of dissolved oxygen and low concentrations of dissolved (bi)sulfide than Raney Ni, suggesting potential for greater catalyst longevity during water treatment applications.



## 1. Introduction

Growing freshwater scarcity is leading many public utilities to use lower quality source waters, including contaminated groundwater and water receiving significant inputs of treated wastewater effluent [1,2]. This raises serious public health concerns about exposure to trace micropollutants present in such source waters [3,4]. These concerns are compounded by the fact that many emerging micropollutants are recalcitrant towards conventional treatment processes [5–7], and new technologies need to be developed to treat these compounds.

*N*-Nitrosamines, including *N*-nitrosodimethylamine (NDMA), have been widely detected in water supplies as a result to contamination from rocket engine testing facilities and as byproducts of wastewater effluent disinfection [5,8–11]. The latter mechanism can also lead to formation of *N*-nitrosamines during disinfection processes at downstream drinking water treatment plants. Although there are currently no federal drinking water regulations for *N*-nitrosamines, public health officials have long recognized that these compounds are potent carcinogens that are much more toxic than the regulated classes of disinfection byproducts [12]. Potential exposure to *N*-nitrosamines has raised concerns about the safety of using drinking water sources that are heavily impacted by wastewater effluent [5].

Non-catalytic and catalytic reductive processes have been investigated as a treatment option for NDMA-contaminated water because the *N*-nitrosamine moiety is susceptible to reductive transformation. Lunn et al. report reduction of NDMA to dimethylamine and/or dimethylhydrazine in water by a variety of metals and metal ions [13,14]. These and other followup studies have shown that Raney Ni (an Al-containing porous Ni material) is especially effective in reducing NDMA under highly basic pH conditions [13–15]. Gillham and co-workers report that granular Fe(0), used to remediate groundwater contaminated with halogenated organic solvents, is also capable of slowly reducing NDMA to dimethylamine and ammonia [16,17]. The addition of Ni surface

* Corresponding author. Tel.: +1 217 244 4679; fax: +1 217 333 6968.
*E-mail address:* strthmnn@uiuc.edu (T.J. Strathmann).

0926-3373/$ – see front matter © 2009 Elsevier B.V. All rights reserved.
doi:10.1016/j.apcatb.2009.03.007

coatings improves Fe(0) reactivity with NDMA, but the enhancement is short-lived [16]. Tests with nanoscale Fe(0) particles containing 0.1 wt.% Pd show that the material is also capable of slowly reducing NDMA over a period of several days [18]. The utility of non-catalytic materials for water treatment is ultimately limited by exhaustion of the metal's reducing equivalents. More recent work shows that NDMA and several other *N*-nitrosamines can be rapidly and catalytically reduced by treatment with hydrogen in combination with supported Pd-based materials or Raney Ni [19–21]. A previous contribution by the authors shows that the metal loading-normalized reactivity of Raney Ni with NDMA exceeds values reported for Pd catalysts [19]. The high activity of Raney Ni and low cost of Ni makes it an attractive alternative to the much more expensive Pd-based catalysts. Unfortunately, Raney Ni is pyrophoric and presents serious safety hazards that limit its use in treatment applications [22]. Furthermore, Raney Ni has been shown to be particularly susceptible to deactivation when exposed to oxidants and reduced sulfur species, even at very low concentrations [19,23].

Several decades after the discovery of Raney Ni [24], Schlesinger et al. reported that reduction of aqueous Ni(II) salts with borohydride yields a stable non-pyrophoric solid containing a mixture of nickel and boron [25]. The composite material (hereafter referred to as NiB) has subsequently been shown to have catalytic reactivity similar to, and sometimes exceeding, that of Raney Ni [26–29]. Several authors have also reported that NiB catalysts have a higher resistance to sulfur fouling than Raney Ni [30–32], critical to their longevity in practical treatment applications. The combination of high activity, stability, and low cost suggests a promising catalytic material for treatment of water contaminated with NDMA and related micropollutants.

The overall goal of this contribution is to provide an initial assessment of the effectiveness of NiB catalysts for the aqueous reduction of NDMA by exogenous hydrogen, and a comparison with commercial Raney Ni catalysts reported on previously [19]. Specific objectives of the study are to: (1) prepare and characterize a NiB catalyst, (2) examine the kinetics and products of NDMA reactions with $H_2$ and the NiB catalyst, (3) quantify the dependence of catalyst activity on catalyst loading and solution pH, and (4) assess the effects of exposure to oxygen and (bi)sulfide catalyst poisons on reactivity with NDMA.

## 2. Experimental

### 2.1. Chemicals

All reagents were of high purity and were used as received from suppliers. NDMA, dimethylamine hydrochloride, 1,1-dimethylhydrazine, 1-fluoro-2,4-dinitrobenzene, 4-nitrobenzaldehyde, $NiCl_2{\cdot}6H_2O$, sodium borohydride ($NaBH_4$), activated Raney Ni (obtained as slurry in water), $Na_2S$, and $NH_4Cl$ were purchased from Sigma–Aldrich. Acetic acid, methanol, acetonitrile, and HCl were purchased from Fisher Scientific. Uniformly $^{15}N$-labeled NDMA was obtained from Cambridge Isotope Laboratories. Ultra high purity hydrogen ($H_2$-99.999%), nitrogen ($N_2$-99.999%), and nitrous oxide ($N_2O$-99.99%) gases were supplied by Matheson Tri Gas. Deionized water (18 MΩ cm; Barnstead NANOpure system) was used to prepare all solutions.

### 2.2. Catalyst preparation

The NiB catalyst was prepared by aqueous reduction of dissolved Ni(II) with borohydride ($BH_4^-$) using procedures modified from earlier reports [25]. All preparation and drying procedures were performed inside an anaerobic glovebox (95% $N_{2(g)}$, 5% $H_{2(g)}$; Pd catalyst changed weekly; Coy Lab Products), and all solutions were prepared with deoxygenated water (boiled and $N_{2(g)}$-sparged for >30 min). A Ni(II) salt solution was prepared by mixing 38.2 g of $NiCl_2{\cdot}6H_2O$ with 1.6 L of water in a 4 L Erlenmeyer flask. A borohydride solution was prepared in a separate 0.5 L Erlenmeyer flask by adding 18.2 g of $NaBH_4$ to 480 mL of water. The borohydride solution was then added stepwise over 1 min to the vigorously mixing Ni(II) solution. A black precipitate and $H_{2(g)}$ evolution was immediately visible. The solution was stirred until $H_{2(g)}$ evolution ceased. The resulting suspension was then filtered (Millipore nylon membrane, 0.45 μm) and the solid catalyst retained on the filter was further rinsed with 1.4 L of water in 0.2 L increments. The catalyst was then dried in a sand bath (115 ± 10 °C) under anoxic conditions for 4 h and stored inside the anaerobic glovebox until used.

The characteristics and catalytic activity of the NiB material were compared with a Raney Ni catalyst reported on previously [19]. The Raney Ni material was obtained from Sigma–Aldrich in a slurry form, and the solid catalyst particles were collected, washed, dried, and stored in the same manner described for the NiB catalyst.

### 2.3. Catalyst characterization

The synthesized NiB catalyst was extensively characterized and compared with the commercial Raney Ni catalyst. The elemental composition was quantified by inductively coupled plasma-mass spectrometry (ICP-MS; Perkin-Elmer SCIEX ELAN DRC-e) following microwave digestion in nitric acid (PerkinElmer/Anton Paar Multiwave 3000). Catalyst surface area and pore structure were determined by collecting $N_{2(g)}$ B.E.T. adsorption–desorption isotherms at 77 K (Micromeritics ASAP 2010 Analyzer); anoxic conditions were maintained during surface area analyses. Bulk crystallinity was determined by powder X-ray diffraction with Cu Kα radiation (Rigaku D-Max-b system), and diffractograms were analyzed with Jade 8.0. The composition and oxidation state of atoms localized at the catalyst surface were determined by X-ray photoelectron spectroscopy using Al Kα radiation (XPS; Physical Electronics PHI 5400). Although tests showed no effects of short-term air exposure, strict anoxic procedures were used to transfer NiB samples into the XPS instrument before placing the samples under vacuum and collecting spectra. From inside the anaerobic glovebox, NiB samples were mounted in an atmospheric isolation chamber that was sealed up before removal from the glovebox and transport to the spectrometer for analysis. XPS spectra were energy-normalized by assigning the carbon 1s peak from the support tape a value of 284.5 eV. Transmission electron micrographs (TEM) were collected with a JEOL 2010 $LaB_6$ system operated at 200 kV, and scanning electron micrographs (SEM) were obtained on a Hitachi S-4700 High Resolution SEM operated at 15 kV.

### 2.4. Kinetic experiments

Kinetic experiments for NiB reactivity with NDMA were conducted using procedures similar to those used for experiments with Raney Ni. Batch experiments were conducted at 25 ± 1 °C in a 300-mL 5-neck round-bottom glass flask immersed in a circulating constant temperature water bath (Thermo Neslab RTE 7). Individual catalyst suspensions were prepared inside an anaerobic glovebox by adding the desired mass of catalyst to a reactor containing 249 mL of deoxygenated water. The reactor was then sealed before removal from the glovebox and connection to a gas sparging system maintained inside a fume hood. The catalyst suspension was then continuously sparged with $H_{2(g)}$ and mixed by magnetic stirring. The gas sparging rate was 0.1 ± 0.01 L $min^{-1}$, and gas was released from the reactor through a mineral oil bubbler that maintained the internal

headspace pressure at 1 atm $H_{2(g)}$ and prevented air intrusion (tests showed no effect of increasing $H_{2(g)}$ sparging rates). A batch kinetics experiment was initiated by injecting 1 mL of NDMA from a concentrated aqueous stock solution into the catalyst suspension. Samples for NDMA analysis were then collected by withdrawing 3 mL aliquots of the suspension with a syringe through a serum-capped stopper on one of the reactor ports, and immediately filtering (0.2 μm Anatop inorganic membrane) to remove catalyst particles and quench the reaction. Unless otherwise stated, reactions were performed at pH 7.0 with a catalyst loading of 500 mg/L, an initial NDMA concentration of 100 μM, and were pre-sparged with $H_{2(g)}$ for 2 h before adding NDMA. Solution pH was maintained with an automated pH-stat controller (Radiometer Titration Manager, TIM854); without pH control, solution pH drifts upward during catalytic NDMA reduction (e.g., drifts from pH 7.0–9.5 when 100 μM NDMA is reduced without pH-stat control).

### 2.5. Analytical methods

NDMA, dimethylamine, and 1,1-dimethylhydrazine were analyzed on a Shimadzu Avp Series high performance liquid chromatograph equipped with a photodiode array detector (HPLC-PDA). A Novapak $C_{18}$ column (150 mm × 3.9 mm, 4 μm packing material) and guard column were used as the stationary phase. An isocratic mobile phase (80% water/20% methanol) with a flow rate of 1 mL $min^{-1}$ was used for NDMA analysis (λ = 226 nm). Dimethylamine and 1,1-dimethylhydrazine were analyzed by HPLC-PDA after derivatization with 1-fluoro-2,4-dinitrobenzene and 4-nitrobenzaldehyde, respectively [33,34]. An isocratic 40/60 mixture of 0.2% acetic acid (pH 4)/methanol (v/v) was used for derivatized dimethylamine samples (λ = 380 nm), and an isocratic 30/70 water/acetonitrile (v/v) mixture was used for derivatized 1,1-dimethylhydrazine samples (λ = 393 nm), both with flow rates of 1 mL $min^{-1}$. Ammonia was analyzed by UV–vis spectrophotometry after derivatization by the phenate method.

Volatile nitrogenous reaction products were quantified by analysis of headspace gas samples collected from crimp-sealed 160-mL serum bottle reactors. Briefly, 35 mg of dry catalyst and 69.5 mL of anoxic water were added to the serum bottle and sealed under anoxic conditions. The solution was then thoroughly sparged with $H_{2(g)}$ to activate the catalyst and remove all $N_2$ from the system. Five and a half mL of a 1.33 mM $H_{2(g)}$-sparged $^{15}N$-labeled NDMA stock solution was then added to the reactor, and headspace samples were collected at selected time intervals by syringe and immediately analyzed by gas chromatography with mass spectrometry detection (Varian 4000 GC/MS). Separation of $H_{2(g)}$, $N_{2(g)}$, and $N_2O_{(g)}$ was achieved on a Varian Plot Fused Silica Coating Molsieve 5A column (25 m × 0.25 mm) with a He carrier gas and isothermal temperature program (300 °C for 5 min). The system was calibrated by equilibrating known masses of unlabeled analytes in sealed serum vials containing the same ratio of water and gas phase as the sealed catalyst suspensions being analyzed, thereby accounting for aqueous-gas partitioning and enabling determination of concentrations in terms of moles of analyte per vial. The batch reaction solutions prepared in the crimp-sealed reactors were initially adjusted to pH 7.0, but pH was not controlled after initiating the reactions.

## 3. Results and discussion

### 3.1. Catalyst characterization

Various properties of the NiB and Raney Ni catalysts are summarized in Table 1, and Fig. 1 shows characterization data for NiB (corresponding data for Raney Ni catalysts provided in Ref. [19]). Elemental analysis reveals that both catalysts contain approximately the same weight percentage of Ni and their corresponding secondary element (i.e., B or Al). The catalyst synthesized for this study contains 85 wt.% Ni, 7 wt.% B, with only traces of sodium (~0.1 wt.%). The remaining catalyst mass is presumed to be mostly oxygen and hydrogen. The composition is similar to earlier reports of nanophase Ni(0) materials synthesized by borohydride reduction [35,36]. The boron content of the NiB materials is slightly higher than that reported for Fe(0) materials [37–39]. The two Ni catalysts differ significantly by their physical surface properties. Raney Ni has roughly five times the specific surface area and four times the pore volume as NiB, whereas the pore diameters of NiB are much larger. The $N_{2(g)}$ adsorption–desorption isotherms for NiB are shown in Fig. 1A. The adsorption isotherm is of type II, according to the Brunauer, Deming, Deming, and Teller classification scheme [40]. Type II isotherms are common for mesoporous materials (pore diameters between 2 nm and 50 nm) [41]. This differs from the type IV isotherm observed for Raney Ni [19], typical of materials that contain micropores with diameter <2 nm [41]. The specific surface area of the NiB particles is similar to earlier reports of NiB materials [42] and nanophase Fe(0) materials synthesized by borohydride reduction [38,43].

**Table 1**
Properties of NiB and Raney Ni catalysts.

| Property | Composition (wt.%) | Specific surface area ($m^2\ g_{cat}^{-1}$) | Pore volume ($cm^3\ g^{-1}$) | Median pore diameter (nm) | Crystallite size (nm) |
|---|---|---|---|---|---|
| NiB | 85% Ni, 7% B | 18 | 0.03 | 20 | 1 |
| Raney Ni | 87% Ni, 8% Al | 100 | 0.11 | 3.4 | 10 |

X-ray diffraction data (Fig. 1B) indicate the presence of metallic Ni phases in NiB with an average crystallite size of 1 nm. This is an order of magnitude smaller than the average size of Ni crystallites in Raney Ni. The small size of the Ni crystallites in NiB is apparent from the broadening of the Ni(1 1 1) diffraction peak.

The XPS spectrum shows that the catalyst surface is composed predominantly of Ni with lesser amounts of O and B. The Ni 2p region of the XPS spectrum (Fig. 1C) shows that Ni exists mostly as elemental Ni(0) at the catalyst surface. The secondary peaks located at slightly higher binding energies are Ni(0) satellite peaks. Surface boron exists as a mixture of elemental and oxidized states (0/+III) (Fig. 1D). The ratio of these two species (as determined by their peak areas) is approximately 30/70 B(0)/B(III). The mixture of B(III) and B(0) species at the material surface is consistent with previous reports for nanophase Ni and Fe materials synthesized by borohydride reduction [35,38,39]. Borohydride ion ($BH_4^-$) is a powerful reducing agent capable of reducing both dissolved Ni(II) and $H_2O$, and several reaction schemes have been proposed for producing Ni(0), B(III), and B(0) in aqueous Ni(II) solutions treated with $BH_4^-$ [44].

XPS results previously reported for the Raney Ni catalyst [19] indicate a similar predominance of Ni(0) at the catalyst surface. However, unlike the NiB catalyst, the secondary aluminum component is not observed in significant amounts at the catalyst surface, indicating a more uniform distribution throughout the Raney Ni structure.

SEM images show that dried NiB forms larger aggregated assemblies of smaller nanoparticles that resemble a porous sponge. The aggregates are generally spherical in shape and vary in size from only a few μm to hundreds of μm. A close-up image of the surface of a NiB aggregate is shown in Fig. 1E. Smaller primary particles are also generally spherical and can be viewed by TEM in Fig. 1F. These primary particles vary from a few nanometers to 100 nm in size. High resolution TEM images also reveal small

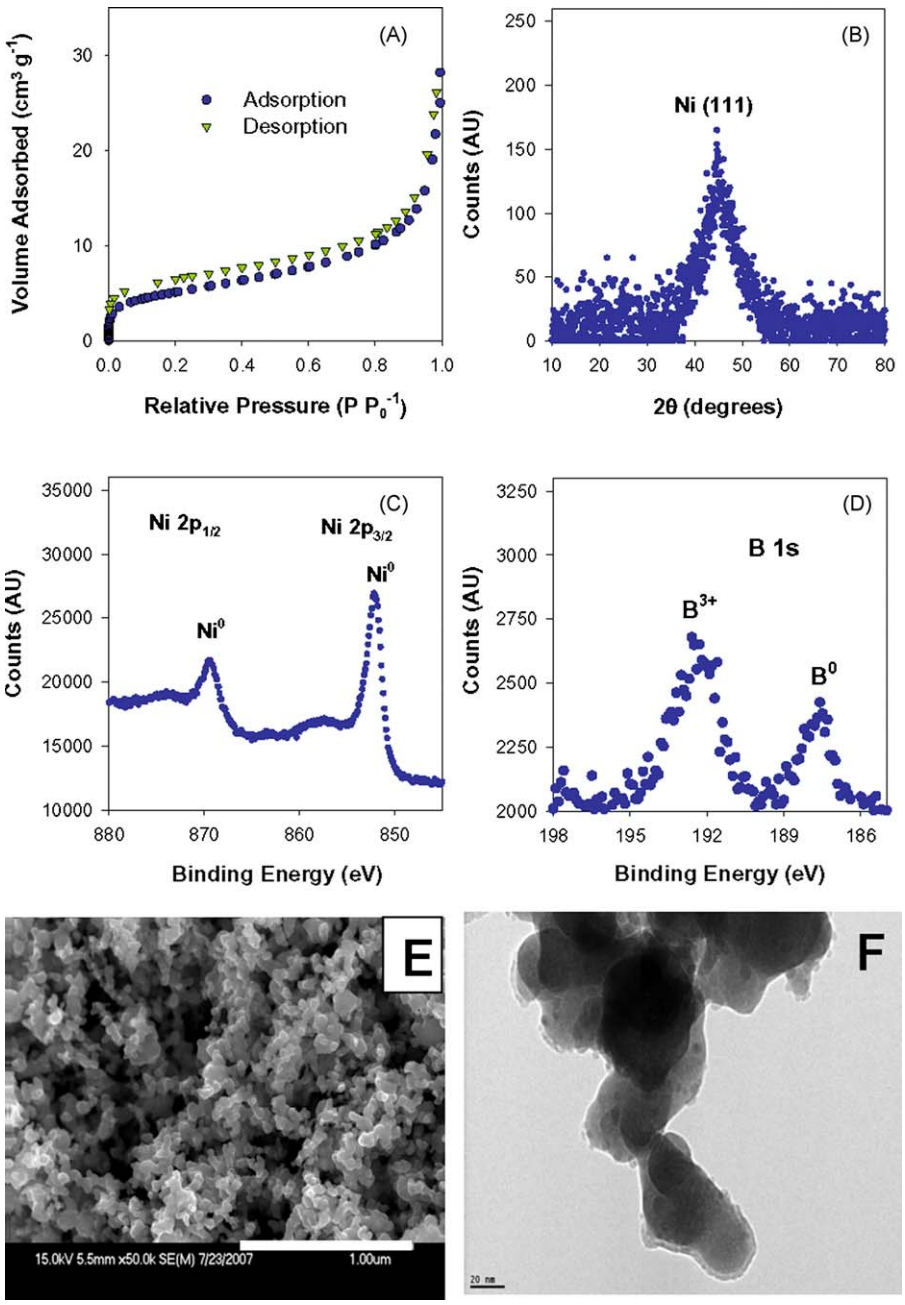


**Fig. 1.** Characterization of the NiB catalyst. (A) $N_{2(g)}$ adsorption–desorption isotherms, (B) powder XRD pattern, (C) Ni 2p region of the XPS spectrum, (D) B 1s region of the XPS spectrum, (E) SEM close-up image of aggregated NiB nanoparticles with 1 μm scale bar, and (F) TEM image of primary NiB particles with 20 nm scale bar.

crystalline regions which vary from less than 1 nm to 2 nm in size, and are believed to be the Ni crystallites observed with X-ray diffraction. Although SEM shows dried aggregates of nanoparticles that are widely ranging in size, further characterization is needed to determine the size of aggregates suspended in aqueous solution, which is most important for assessing reactivity (preliminary dynamic light scattering measurements indicate the presence of smaller aggregates 100 nm to 5 μm in size). For a more detailed description of the fine nanostructure of NiB, refer to Geng et al. [45].

### 3.2. NDMA reduction kinetics and products

Investigation of NiB catalyst activity show that NDMA is rapidly reduced in the presence of the catalyst and $H_2$, yielding dimethylamine and ammonia according to the following stoichiometry, consistent with oxidation of 3 equivalents of $H_2$:

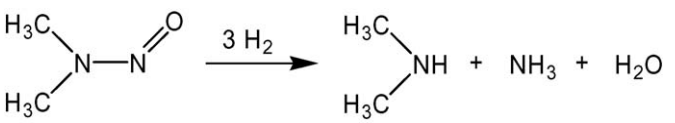


(1)

Fig. 2 shows a typical reaction time course for reduction of NDMA by NiB. NDMA disappearance in batch reactions follows a pseudo first-order rate law as indicated by the model fit provided, and the reaction half life is only 2.2 min under the conditions shown. Dimethylamine formation occurs with no lag time, as indicated by

the steady carbon mass balance. The nitrogen mass balance exhibits a very small dip at early reaction times due to a small lag in ammonia formation, but otherwise is close to 100% throughout the course of the reaction. None of the potential gaseous products of the reaction (e.g., $^{15}N_2$, $^{15}N_2O$) were detected with GC–MS in experiments using uniformly $^{15}N$-labeled NDMA. Such products would have been readily detected at analyte concentrations used in this study. Thus, the total mass balance can be closed using dimethylamine and ammonia alone. These results differ from findings reported for reactions with Raney Ni [19]. Although dimethylamine formation is observed with both catalysts, $N_2$ is observed in place of ammonia when NDMA is reduced with the Raney Ni catalyst, consistent with oxidation of 1.5 equivalents of $H_2$:

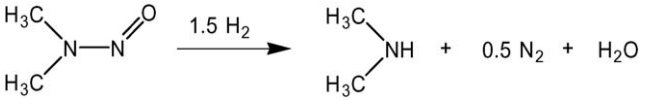


(2)

An additional test confirms that the NiB material acts to catalyze the reduction of NDMA by exogenous $H_{2(g)}$, rather than acting as a non-catalytic stoichiometric reductant. NDMA reduction in a $H_2$-saturated suspension of NiB was demonstrated at conditions where NDMA was initially present in significant stoichiometric excess of the theoretical reducing equivalents available from Ni(0) and B(0) (4 mM NDMA reduced in a suspension containing 100 mg/L NiB, which contains only ~20% of the required reducing equivalents in Eq. (1) if Ni(0) is oxidized to Ni(II), and if B(0) is oxidized to B(III)).

### 3.3. Proposed reaction mechanism

Experimental results with the NiB catalyst are consistent with a surface-mediated reaction mechanism initiated by scission of the molecular hydrogen H–H bond to form two equivalents of adsorbed atomic hydrogen (≡Ni–$H_{ads}$) (Eq. (3)) and dissociation of the *N*-nitrosamine N–N bond to form adsorbed $N(CH_3)_2$ and NO fragments (Eq. (4)):

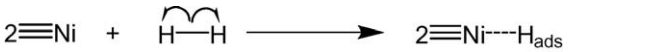


(3)

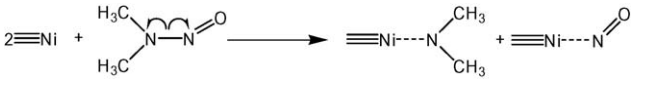


(4)

The two nitrogen fragments subsequently react with $H_{ads}$ to form the observed products of dimethylamine and ammonia (Eqs. (5) and (6)):

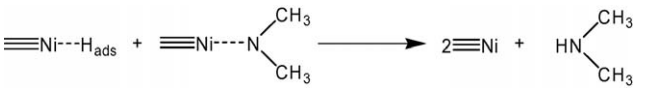


(5)


(6)

Note that Eq. (6) represents a multi-step process and is not meant to indicate a single elementary reaction step. As mentioned above, the ammonia replaces the $N_2$ product observed for reactions with Raney Ni. Ammonia has also been reported as the product of NDMA reduction with Ni-coated zerovalent iron and supported Pd catalysts [16,20,21]. The mechanism controlling the final NDMA reduction product distribution with the two Ni catalysts is unclear and likely affected by complex heterogeneous processes. One possible explanation for the differing products could be varying lifetimes of the N═O fragments on different catalyst surfaces prior to being reduced. B(0)/B(III) deposits on the NiB surface, which are estimated from elemental composition to account for roughly 25 atom% of the catalyst surface (and possibly more if boron is elevated at the surface like it is in nanophase Fe(0) [39]), could slow diffusion of N═O fragments across the surface and inhibit N–N pairing reactions that are critical to $N_2$ formation [46]. Nurmi et al. suggested that varying product distributions observed for carbon tetrachloride reactions with different nanoscale Fe(0) materials may be due, at least in part, to the presence versus absence of surface boron deposits on the materials [38]. Regardless, the final products are much less toxic than the parent *N*-nitrosamine, and at typical levels of NDMA water contamination (<1 μg/L [47]) these products are expected to be formed at concentrations much lower than background levels.

Some earlier studies have proposed that NDMA is reduced by an alternative pathway in which the N═O bond in NDMA is initially cleaved to form 1,1-dimethylhydrazine as a reaction intermediate that is subsequently reduced to dimethylamine and ammonia [13,15]. Tests here show that 1,1-dimethylhydrazine is reduced to dimethylamine and ammonia by the NiB catalyst, but at a much lower rate compared with NDMA at the same conditions ($k_{obs} \approx 25\%$ of $k_{obs}$ measured for NDMA). Thus, if 1,1-dimethylhydrazine is being formed as an intermediate during the reduction of NDMA, it should build up to detectable levels in solution and delay the formation of dimethylamine and ammonia markedly. However, no 1,1-dimethylhydrazine is observed during NDMA reactions and there is no significant lag in the final product formation, demonstrating that 1,1-dimethylhydrazine is not an intermediate in the major reduction pathway for NDMA with NiB.

### 3.4. Effect of catalyst loading on reaction kinetics

A series of kinetic experiments were conducted to assess the influence of catalyst loading and solution pH on reaction rates. Fig. 3A and B shows the measured pseudo first-order rate constants for NDMA reduction by Raney Ni and NiB catalysts as a function of catalyst loading plotted in terms of catalyst mass (grams of Ni per liter of suspension) and catalyst surface area (square meters of catalyst surface area per liter of suspension), respectively. The plots show that reaction rates are linearly dependent on the amount of NiB and Raney Ni catalyst present in suspension. This finding demonstrates that the observed reaction rates are not $H_2$-limited, and it enables a comparison of the activity of NiB with Raney Ni in terms of applied catalyst mass and the apparent surface area.

Mass- and surface area-normalized rate constants ($k_{cat,m}$ and $k_{cat,sa}$) for NDMA reduction can be determined by linear regression of the measured rate constants in Fig. 3A and B, respectively. Analysis of the data in Fig. 3A yields $k_{cat,m}$ values of $77.9 \pm 13.1$ L $g_{Ni}^{-1}$ $h^{-1}$ and $29.5 \pm 2.4$ L $g_{Ni}^{-1}$ $h^{-1}$ for Raney Ni and NiB, respectively (uncertainty represents 95% confidence level). Thus, the current NiB catalyst is less active than Raney Ni on a mass-normalized basis. However, analysis of data in Fig. 3B shows that the NiB catalyst is more active than Raney Ni when reactivity is normalized by B.E.T. surface area. Linear regression yields $k_{cat,sa}$ values of $0.68 \pm 0.11$ L $m_{cat}^{-2}$ $h^{-1}$ and $1.38 \pm 0.11$ L $m_{cat}^{-2}$ $h^{-1}$ for Raney Ni and NiB, respectively. This finding suggests that the NiB surface sites have a higher intrinsic reactivity with NDMA than Raney Ni, if it can be assumed that the exposed surface areas of each catalyst

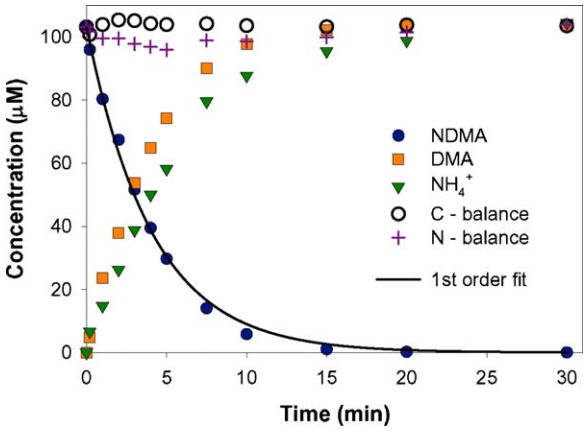


**Fig. 2.** NDMA reduction by $H_2$ in water containing NiB catalyst. Reaction conditions: 100 μM NDMA, 500 mg/L NiB, $P_{H_2}$ = 1 atm, pH 7.0, and 25 °C. First-order rate law fit yields an observed rate constant, $k_{obs}$ = 3.15(±0.17) × $10^{-1}$ $min^{-1}$. Uncertainty provided at the 95% confidence level.

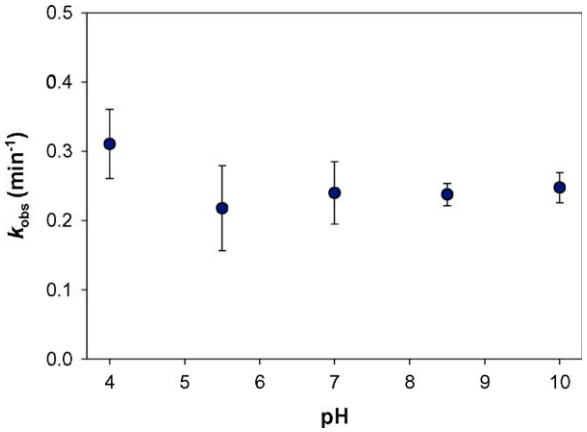


**Fig. 4.** Effect of solution pH on the rate constant for NDMA reduction with NiB catalyst. Reaction conditions: 500 mg/L NiB $[NDMA]_{init}$ = 100 μM, $P_{H_2}$ = 1 atm, and 25 °C. Error bars represent triplicate-averaged standard deviations.

that are available for NDMA reactions are consistent with the B.E.T. specific surface area measurements. However, the validity of this assumption is unclear because Ni catalyst nanoparticles, like most nanoparticles, are present in solution in an aggregated form, potentially limiting the available surface area for reactions with NDMA. Preliminary dynamic light scattering measurements indicate the presence of some aggregates ranging in size from 100 nm to 5 μm, but further studies are needed to address the influence of nanoparticle aggregation to NiB catalyst reactivity with aqueous contaminants.

Although aggregation of the primary nanoparticles of NiB may limit the fraction of surface sites available for reactions with NDMA, kinetic tests and calculations indicate that aggregation does not lead to a significant intraparticle mass transfer limitation to NDMA reactions with the catalyst. First, the mass-normalized rate constant for NDMA reduction by catalyst aggregates <60 μm in size (sieved) was found to be similar to the rate constant measured with unfractionated NiB, which contains many dried aggregates >100 μm in size (from SEM analysis). If reactivity of the NiB aggregates is limited by mass-transfer through the porous aggregate, we would expect greater reactivity of the <60 μm size fraction of NiB catalyst, but this is not the case. Furthermore, comparison of characteristic timescales for diffusion of NDMA through a hypothetical 60 μm porous particle relative to the characteristic timescale observed for the reaction [48–50] indicates that the reaction is much slower than intraparticle diffusion, supporting a conclusion that the kinetics for catalytic reduction of NDMA are under surface chemical reaction control (detailed calculation for Raney Ni provided in the Supporting Information section of Ref. [19]).

It is also worth noting here that the mass-normalized rate constants for NDMA reduction by Raney Ni and NiB compare favorably with rate constants measured by Davie et al. for $Al_2O_3$-supported 1% Pd (11.5 L $g_{Pd}^{-1}$ $h^{-1}$), 1% Pd–0.3% Cu (66.5 L $g_{Pd}^{-1}$ $h^{-1}$), and 5% Pd–1% In (46.8 L $g_{Pd}^{-1}$ $h^{-1}$) catalysts [20,21]. This is of practical relevance because non-precious metals like Ni are much cheaper than Pd and other noble metals used for catalytic applications.

### 3.5. Effect of pH on reaction kinetics

It is important to assess the stability of catalytic reduction processes in natural waters and water treatment systems with varying pH conditions. Kinetic experiments show no significant effect of varying pH from 4 to 10 on the reactivity of NDMA with the NiB catalyst (Fig. 4). The lack of an observed pH effect agrees with the trend observed for NDMA reaction with the Raney Ni catalyst [19]. Together, these finding indicate that the reactivity of $H_{ads}$ at metal catalyst surfaces is not directly affected by the pH of the contacting solution.

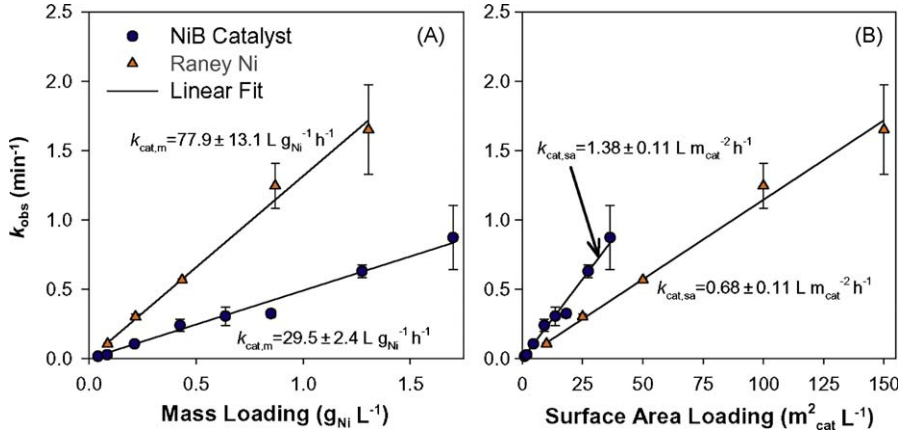


**Fig. 3.** Pseudo first-order rate constants for NDMA reduction in suspensions containing varying amounts of NiB and Raney Ni catalysts ($[NDMA]_{init}$ = 100 μM, $P_{H_2}$ = 1 atm, pH 7.0, and 25 °C). Catalyst loading is represented in terms of (A) mass of Ni per liter of suspension and (B) catalyst surface area per liter of suspension. Error bars for NiB represent standard deviations for triplicate reactions (smaller than symbol if not shown). Data for Raney Ni from Ref. [19].

### 3.6. Stability of Ni catalysts in the presence of oxygen

As stated in the introduction, NiB materials are reported to be non-pyrophoric when exposed to air [26], which, if true, would be advantageous in comparison to Raney Ni catalysts. Pyrophoric materials present serious safety hazards and must be handled with extreme care and often only with specialized equipment. Unlike Raney Ni, the NiB catalyst prepared for this study shows no apparent pyrophoric properties and resists oxidation when the dry catalyst is exposed to air for extended periods of time. Fig. 5A shows pseudo first-order rate constants for NDMA reduction with Raney Ni and NiB catalysts measured after pre-exposing the dry catalyst to air for different time periods before adding to $H_2$-saturated aqueous solutions and measuring the rate of NDMA reduction using the same procedure described in Section 2. Comparing the first two bars shows that the Raney Ni loses all activity towards NDMA reduction when the dry catalyst is exposed to air (ambient laboratory room conditions) for even a very short period of time (safety note: Raney Ni catalyst was slowly dosed with air to avoid excess heat generation and combustion resulting from catalyst oxidation). The loss in catalyst activity results from Ni(0) oxidation by $O_{2(g)}$. XPS measurements of Raney Ni after $t_{air}$ = 1 h show that surface Ni(0) has been completely oxidized to Ni(II), which is catalytically inactive. In addition, separate tests show that Ni(0) oxidation is accompanied by significant reductions in both the specific surface area and pore volume of catalyst. In contrast to Raney Ni, the activity of the NiB catalyst is unaffected when the dry catalyst is exposed to air for extended lengths of time (up to $t_{air}$ = 110 days in this study) before measuring reactivity with NDMA. In contrast to the Raney Ni, XPS measurements of NiB at $t_{air}$ = 1 h show a continued predominance of Ni(0) at the catalyst surface. Instead, XPS measurements show that NiB catalyst exposure to air oxidizes surface B(0) to B(III) (Fig. 6). This appears to have no apparent effect on catalyst activity, indicating that surface B plays a protective, but non-catalytic role. The stability of NiB in air indicates that the catalyst can be stored and shipped safely under ambient conditions, providing a major practical advantage over Raney Ni.

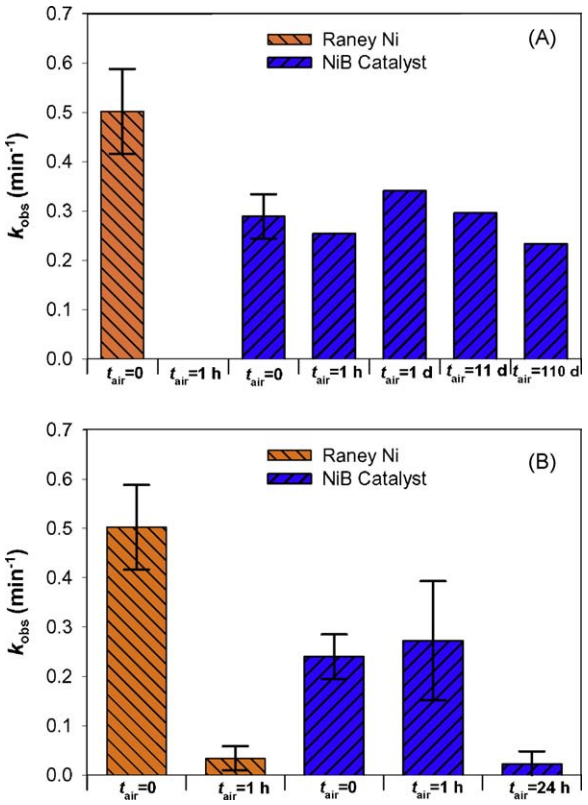


**Fig. 5.** Air-tolerance of NiB and Raney Ni catalysts. (A) Effects of exposing dry Ni catalysts to air for different lengths of time ($t_{air}$) prior to measuring catalyst reactivity with NDMA. (B) Effects of exposing Ni catalysts to air-saturated water (suspension continuously sparged with air) for different lengths of time prior to measuring reactivity with NDMA. After exposing catalysts to air, catalyst suspensions were sparged with $H_{2(g)}$ before introducing NDMA. Reaction conditions: 500 mg/L catalyst $[NDMA]_{init}$ = 100 μM, pH 7.0, $P_{H_2}$ = 1 atm, and 25 °C. Error bars represent triplicate-averaged standard deviations.

Fig. 5B shows how catalyst activity is affected after exposing the catalysts to air-saturated water. In these experiments, aqueous suspensions of Raney Ni and NiB catalysts were sparged with air for 1 h before switching to $H_{2(g)}$ sparge and conducting a batch reaction with NDMA using procedures outlined in Section 2. The $k_{obs}$ values for NDMA reduction by virgin catalysts maintained under strict anoxic conditions are shown for comparison. Results of these experiments show that the activity of Raney Ni is severely diminished following exposure to air-saturated water containing ~250 μM dissolved oxygen, whereas the activity of NiB remains unchanged following short-term exposure to air-saturated water. Longer term exposure ($t_{air}$ = 24 h) of NiB to air-saturated water eventually deactivates the catalyst, indicating that NiB is not completely immune to dissolved oxygen. Nevertheless, the results demonstrate that the NiB catalyst has a far greater capacity to resist oxidation than Raney Ni.

### 3.7. Stability of Ni catalysts in the presence of (bi)sulfide

Resistance to sulfur poisoning is desirable for improving catalyst longevity. Reduced sulfur species are well known to deactivate Ni and Pd catalysts by strong chemisorption to the active surface sites [19,23,51], thereby limiting their use for treating waters with even low levels of reduced sulfur. Fig. 7 shows the results of experiments designed to assess the effects of (bi)sulfide on Ni catalyst activity. The plot shows pseudo first-order rate constants for NDMA reduction with NiB and Raney Ni catalysts in the absence and presence of various concentrations of (bi)sulfide. To accurately compare the effects of (bi)sulfide on the activity of the two catalysts, all reactors were prepared with equivalent catalyst surface area loading (50 $m^2_{cat}$ $L^{-1}$).

For Raney Ni, when catalyst suspensions are amended with 0.1 mM, 1 mM, and 10 mM (bi)sulfide, there are significant and progressive losses of activity (even at the lowest concentration examined), until the catalyst is completely deactivated by 10 mM (bi)sulfide [19]. For NiB, the trend is similar at higher (bi)sulfide

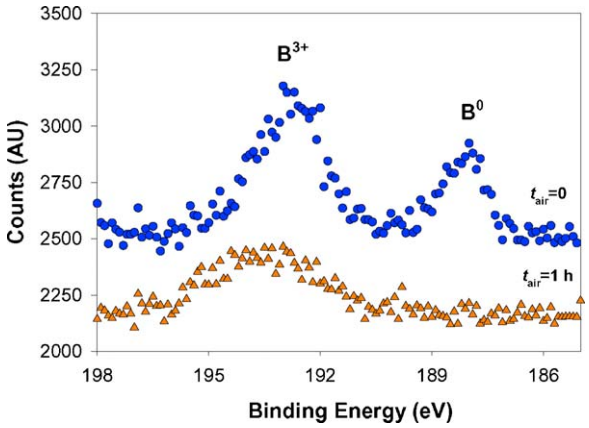


**Fig. 6.** Effect of NiB exposure to air on boron surface species. B 1s region of XPS spectra of virgin NiB maintained under anoxic conditions in comparison to NiB exposed to air for 1 h. Ni 2p region of the same spectra shows no effect of air exposure on surface Ni speciation.

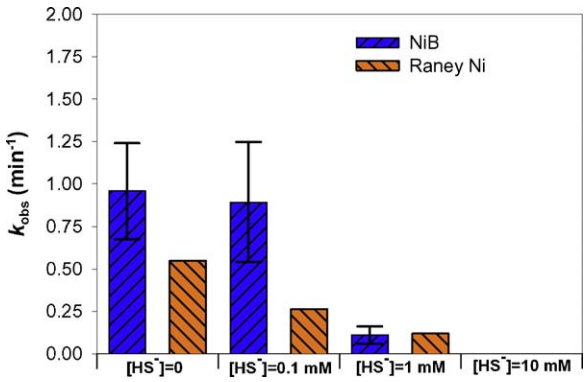


**Fig. 7.** (Bi)sulfide tolerance of Ni catalysts. Ni catalysts are exposed to varying concentrations of (bi)sulfide during catalyst reactions with NDMA. (Bi)sulfide is injected into the reactor simultaneously with NDMA. Reaction conditions: 50 $m^2_{cat}$ $L^{-1}$ Ni catalyst $[NDMA]_{init}$ = 100 μM, pH 7.0, $P_{H_2}$ = 1 atm, and 25 °C. Error bars for NiB represent triplicate-averaged standard deviations. Data for Raney Ni from Ref. [19].

concentrations, but no loss in catalyst activity is observed in suspension amended with 0.1 mM (bi)sulfide. XPS measurements suggest that the observed deactivation of Raney Ni catalysts results from strong chemisorption of (bi)sulfide species to the catalyst surface and conversion of Ni(0) catalytic sites to inactive Ni(II)S surface sites [19].

The resistance of NiB to low levels of (bi)sulfide has been observed previously for similar NiB composite materials and has been attributed to the ability of B(0) to preferentially adsorb (bi)sulfide, leaving the catalytically active Ni(0) unaffected [31]. It has been hypothesized that this occurs due to electron donor–acceptor interactions between Ni(0) and B(0). XPS studies show that B(0) donates electron density to Ni(0), leaving the boron electron deficient and increasing its affinity for (bi)sulfide [29,31,42,52]. Density functional theory calculations also show that (bi)sulfide preferentially binds to B over Ni in simulated NiB clusters [32]. Earlier studies also suggest that (bi)sulfide binding to B is a reversible process [31], so low (bi)sulfide concentrations would not build up on NiB surfaces. Exposure to higher (bi)sulfide concentrations eventually overwhelms the available B sites and spills over to Ni(0) catalyst sites, leading to catalyst deactivation. In-depth spectroscopy studies are needed to further investigate sulfide interactions with NiB surfaces at different concentrations and characterize the mechanisms responsible for the catalyst's resistance to sulfide poisoning.

Although Fig. 7 shows that NiB is deactivated by exposure to high concentrations of (bi)sulfide, it should be kept in mind that the higher tested (bi)sulfide concentrations are much greater than typical concentrations in natural water matrices (with the possible exception of groundwater from highly sulfate-reducing environments). Therefore, the low concentrations of reduced sulfur in natural waters may not adversely affect the activity of NiB over extended periods of time. However, long-term studies with flow-through reactors that better represent real treatment systems are needed to appropriately assess catalyst longevity in the presence of low levels of reduced sulfur species, oxygen and other potential catalyst foulants.

## 4. Conclusions

In conclusion, the reduction of aqueous Ni(II) with sodium borohydride yields a non-pyrophoric nanophase NiB hydrogenation catalyst that has high reactivity with NDMA, a toxic byproduct of water disinfection processes and groundwater contaminant near aerospace facilities. Catalytic treatment of NDMA yields stoichiometric amounts of dimethylamine and ammonia, which are much less toxic than NDMA and are likely to be formed at very low concentrations (e.g., <1 μg/L [5]) that are below their natural background levels in most treatment applications. Kinetic studies show that NiB catalyst reactivity with NDMA is independent of pH, and long-term exposure of the dry catalyst in air, as well as short-term exposure of the suspended catalyst to dissolved oxygen, have little effect on catalyst activity. The NiB catalyst also shows a greater tolerance to reduced sulfur than Raney Ni, exhibiting no apparent loss in reactivity with NDMA in suspensions amended with 0.1 mM (bi)sulfide. These findings, combined with the much lower cost of Ni compared to Pd and other precious metal catalysts, suggest that NiB catalysts may be promising candidates for treatment technology development. The stability of NiB in air is particularly important because it will allow for safe storage, shipment, and handling unlike, Raney Ni. In addition, the tolerance to low levels of dissolved oxygen and (bi)sulfide is critical, because low concentrations can be expected even when taking great care to exclude these substances from reactor feedwater.

Although NiB is a promising catalyst, further research is needed to address a number of issues before the material can be practically implemented for water treatment applications. First, additional research may lead to further improvements in NiB catalyst activity. Findings from this study show that, when normalized by B.E.T. surface area, the NiB catalyst exhibits greater reactivity with NDMA than previously studied pyrophoric Raney Ni catalysts. However, the as-synthesized NiB nanoparticles form aggregates of indeterminate size in water that may limit the availability of surface sites for reactions with aqueous contaminants. The precise influence NiB nanoparticle aggregation has on reaction kinetics remains unclear and warrants further in-depth study. It is likely that surface site availability, and hence catalyst activity, can be markedly improved by dispersing NiB nanoparticles on inert support materials.

In addition to improvements in the activity of NiB catalysts, extensive studies are needed to evaluate the long-term stability and sustainability of NiB catalysts when treating NDMA in complex matrices (e.g., contaminated groundwater, disinfected wastewater effluent) in more realistic flow-through pilot reactors (e.g., packed column systems). Quantifying catalyst effectiveness and catalyst longevity during treatment is necessary to compare treatment costs with competing technologies. Improvements in catalyst longevity will also benefit from research on the mechanisms responsible for catalyst fouling and deactivation, as well as methods for regenerating fouled catalysts. In addition to ensuring sustained catalyst activity, careful analysis of the potential for leaching of dissolved Ni and B or release of NiB nanoparticles from the catalyst aggregates needs to be performed during treatment. Although not currently regulated, both of these substances are water contaminants of concern, and recent studies suggest toxic effects of exposure to nanoparticles in general [53–55]. Thus, minimal leaching and nanoparticle release are a prerequisite for use of NiB catalysts in water treatment applications. Furthermore, rapid leaching of these substances would drastically reduce the catalyst lifetime, leading to increased treatment costs and reduced practicality. Ultimately, achieving low treatment costs, maintaining long-term catalyst activity, and minimizing the leaching of catalyst materials are mutually dependent requirements for widespread adoption of catalytic water treatment technologies.

## Acknowledgments

This work was supported by the National Science Foundation through WaterCAMPWS, a Science and Technology Center of Advanced Materials for the Purification of Water with Systems (CTS-0120978) and funding provided by the Division of Chemical,

Bioengineering, Environmental, and Transport Systems (CBET 07-46453 CAREER). XRD, XPS, TEM, and SEM analyses were performed at the Center for Microanalysis of Materials, University of Illinois, which is partially supported by the U.S. Department of Energy under grant DEFG02-91-ER45439. Experimental assistance and valuable insights were provided by John Shapley, Charles Werth, Tias Paul, Kathryn Guy, Rick Haasch, Jim Mabon, Mauro Sardela (Univ. Illinois), and two anonymous reviewers.

## References

[1] D.A. Okun, Annu. Rev. Public Health 21 (2000) 223–245.
[2] D.L. Sedlak, J.L. Gray, K.E. Pinkston, Environ. Sci. Technol. 34 (2000) 508A–515A.
[3] S.A. Snyder, P. Westerhoff, Y. Yoon, D.L. Sedlak, Environ. Eng. Sci. 20 (2003) 449–469.
[4] C.G. Daughton, T.A. Ternes, Environ. Health Perspect. 107 (1999) 907–938.
[5] W.A. Mitch, J.O. Sharp, R.R. Trussell, R.L. Valentine, L. Alvarez-Cohen, D.L. Sedlak, Environ. Eng. Sci. 20 (2003) 389–404.
[6] T.A. Ternes, R. Hirsch, Environ. Sci. Technol. 34 (2000) 2741–2748.
[7] T.A. Ternes, M. Meisenheimer, D. McDowell, F. Sacher, H.J. Brauch, B. Haiste-Gulde, G. Preuss, W. Wilme, N. Zulei-Seibert, Environ. Sci. Technol. 36 (2002) 3855–3863.
[8] R.L. Tate, M. Alexander, J. Environ. Qual. 5 (1976) 131–133.
[9] D. Gunnison, M.E. Zappi, C. Teeter, J.C. Pennington, R. Bajpai, J. Hazard. Mater. 73 (2000) 179–197.
[10] W.C. Yang, J. Gan, W.P. Liu, R. Green, J. Environ. Qual. 34 (2005) 336–341.
[11] W.A. Mitch, G.L. Oelker, E.L. Hawley, R.A. Deeb, D.L. Sedlak, Environ. Eng. Sci. 22 (2005) 882–890.
[12] United States Environmental Protection Agency (USEPA), Ambient water quality criteria for nitrosamines, Office of Water Regulations and Standards Criteria and Standards Division, Washington, DC, 1980, EPA 440/5-80-064, in: W.D. Office of Water Regulations and Standards Criteria and Standards Division (Ed.), 1980.
[13] G. Lunn, E.B. Sansone, L.K. Keefer, Carcinogenesis 4 (1983) 315–319.
[14] G. Lunn, E.B. Sansone, Environ. Sci. Technol. 17 (1983) 240–243.
[15] B. Greene, M.B. McClure, H.T. Johnson, Chem. Health Saf. 11 (January/February) (2004) 6–13.
[16] L. Gui, R.W. Gillham, M.S. Odziemkowski, Environ. Sci. Technol. 34 (2000) 3489–3494.
[17] M.S. Odziemkowski, L. Gui, R.W. Gillham, Environ. Sci. Technol. 34 (2000) 3495–3500.
[18] C.E. Schaefer, C. Topoleski, M.E. Fuller, Water Environ. Res. 79 (2007) 57–62.
[19] A.J. Frierdich, J.R. Shapley, T.J. Strathmann, Environ. Sci. Technol. 42 (2008) 262–269.
[20] M.G. Davie, M. Reinhard, J.R. Shapley, Environ. Sci. Technol. 40 (2006) 7329–7335.
[21] M. Davie, K. Shih, F. Pacheco, J. Leckie, M. Reinhard, Environ. Sci. Technol. 42 (2008) 3040–3046.
[22] J. Petró, A. Bóto, K. László, H. Beyer, E. Kálmán, I. Dódony, Appl. Catal. A 190 (2000) 73–86.
[23] R.D. Kelley, G.A. Candela, T.E. Madey, D.E. Newbury, R.R. Schehl, J. Catal. 80 (1983) 235–248.
[24] M. Raney, Method of Producing Finely-divided Nickel, US Patent (1927).
[25] H.I. Schlesinger, H.C. Brown, A.E. Finholt, J.R. Gilbreath, H.R. Hoekstra, E.K. Hyde, J. Am. Chem. Soc. 75 (1953) 215–219.
[26] C.A. Brown, H.C. Brown, J. Am. Chem. Soc. 85 (1963) 1003–1005.
[27] C.A. Brown, J. Org. Chem. 35 (1970) 1900–1904.
[28] C.A. Brown, V.K. Ahuja, J. Org. Chem. 38 (1972) 2226–2230.
[29] H. Li, H. Li, W. Dai, M. Qiao, Appl. Catal. A 235 (2003) 119–130.
[30] C.H. Bartholomew, A.H. Uken, Appl. Catal. 4 (1982) 19–29.
[31] W.J. Wang, H.X. Li, J. Deng, Appl. Catal. A 203 (2000) 293–300.
[32] C. Luo, W.N. Wang, M.H. Qiao, K.N. Fan, J. Mol. Catal. 184 (2002) 379–386.
[33] R.W. Gillham, L. Gui, M.S. Odziemkowski, Environ. Sci. Technol. 34 (2000) 3489–3494.
[34] A.A. Denisov, A.D. Smolenkov, O.A. Shpigun, J. Anal. Chem. 59 (2004) 452–456.
[35] H. Li, H. Li, W. Dai, M. Qiao, Appl. Catal. A 238 (2003) 119–130.
[36] P.C. Maybury, R.W. Mitchell, M.F. Hawthorne, J. Chem. Soc. Chem. Commun. (1974) 534–535.
[37] Y. Liu, S.A. Majetich, R.D. Tilton, D.S. Sholl, G.V. Lowry, Environ. Sci. Technol. 39 (2005) 1338–1345.
[38] J.T. Nurmi, P.G. Tratnyek, V. Sarathy, D.R. Baer, J.E. Amonette, K. Pecher, C.-y. Wang, J.C. Linehan, D.W. Matson, R.L. Penn, M.D. Driessen, Environ. Sci. Technol. 39 (2005) 1221–1230.
[39] S.M. Ponder, J.G. Darab, J. Bucher, D. Caulder, I. Craig, L. Davis, N. Edelstein, W. Lukens, H. Nitsche, L. Rao, D.K. Shuh, T.E. Mallouk, Chem. Mater. 13 (2001) 479–486.
[40] S. Brunauer, L.S. Deming, W.S. Deming, E. Teller, J. Am. Chem. Soc. 62 (1940) 1723–1732.
[41] S. Lowell, Introduction to Powder Surface Area, Wiley Interscience, New York, 1979.
[42] H. Li, H. Luo, L. Zhang, W. Dai, M. Qiao, J. Mol. Catal. A 203 (2003) 267–275.
[43] B.H. Liu, Z.P. Li, S. Suda, J. Alloys Compd. 415 (2006) 288–293.
[44] J. Shen, Z.T. Li, Q. Yan, Y. Chen, J. Phys. Chem. 97 (1993) 8504–8511.
[45] J. Geng, D.A. Jefferson, B.F. Johnson, Chem. Commun. (2007) 969–971.
[46] K.-D. Vorlop, U. Prüsse, in: F.J.J. Janssen, R.A. van Santen (Eds.), Environmental Catalysis, Imperial College Press, London, 1999, pp. 195–218.
[47] E. Pehlivanoglu-Mantas, E.L. Hawley, R.A. Deeb, D.L. Sedlak, Water Res. 40 (2006) 341–347.
[48] P.B. Weisz, C.D. Prater, Adv. Catal. 6 (1954) 143.
[49] C.N. Satterfield, Mass Transfer in Heterogeneous Catalysis, MIT Press, Cambridge, MA, 1969.
[50] O. Levenspiel, Chemical Reaction Engineering, Wiley, New York, 1972.
[51] B.P. Chaplin, E. Roundy, K.A. Guy, J.R. Shapley, C.J. Werth, Environ. Sci. Technol. 40 (2006) 3075–3081.
[52] H. Li, H. Li, W.-L. Dai, W. Wang, Z. Fang, J.-F. Deng, Appl. Surf. Sci. 152 (1999) 25–34.
[53] M. Cempel, G. Nikel, Pol. J. Environ. Stud. 15 (2006) 375–382.
[54] J.L. Parks, M. Edwards, Environ. Sci. Technol. 35 (2005) 81–114.
[55] R.J. Griffitt, J. Luo, J. Gao, J.C. Bonzongo, D.S. Barber, Environ. Toxicol. Chem. 27 (2008) 1972–1978.